

Controlled propagation and particle manipulation of off-axis-rotating elliptical Gaussian beams in strong nonlocal media

Rong-Quan Chen(陈荣泉), Rui-Lin Xiao(肖瑞林), Wei Wang(王伟), Xi-Xi Chu(储茜茜), Yu-Qing Song(宋雨晴), Xu-Dong Hu(胡旭东), and Ming Chen(陈明)

Citation: Chin. Phys. B, 2025, 34 (**3**): 034205. DOI: 10.1088/1674-1056/ada9dd
Journal homepage: http://cpb.iphy.ac.cn; http://iopscience.iop.org/cpb

What follows is a list of articles you may be interested in

Four-wave mixing Bragg scattering for small frequency shift from silicon coupled microrings

Chang Zhao(赵畅), Chao Wu(吴超), Pingyu Zhu(朱枰谕), Yuxing Du(杜昱星), Yan Wang(王焱), Miaomiao Yu(余苗苗), Kaikai Zhang(张凯凯), and Ping Xu(徐平)
Chin. Phys. B, 2025, 34 (**1**): 014206. DOI: 10.1088/1674-1056/ad8a4f

Manganese dioxide as wide adaptive ultrafast photonic device for pulsed laser generation

Xin-He Dou(窦鑫河), Zhen Chen(陈震), Chen-Yan Zhang(张辰妍), Xiang Li(李响), Fei-Hong Qiao(乔飞鸿), Bo-Le Song(宋博乐), Shan Wang(王珊), Hao Teng(滕浩), and Zhi-Guo Lv(吕志国)
Chin. Phys. B, 2024, 33 (**11**): 114202. DOI: 10.1088/1674-1056/ad71b5

Plasmon-induced nonlinear response on gold nanoclusters

Yuhui Song(宋玉慧), Yifei Cao(曹逸飞), Sichen Huang(黄思晨), Kaichao Li(李凯超), Ruhai Du(杜如海), Lei Yan(严蕾), Zhengkun Fu(付正坤), and Zhenglong Zhang(张正龙)
Chin. Phys. B, 2024, 33 (**4**): 044204. DOI: 10.1088/1674-1056/ad1a8b

Using harmonic beam combining to generate pulse-burst in nonlinear optical laser

Yuan-Zhai Xu(许元斋), Zhen-Ling Li(李珍玲), Ao-Nan Zhang(张奥楠), Ke Liu(刘可), Jing-Jing Zhang(张晶晶), Xiao-Jun Wang(王小军), Qin-Jun Peng(彭钦军), and Zu-Yan Xu(许祖彦)
Chin. Phys. B, 2024, 33 (**1**): 014206. DOI: 10.1088/1674-1056/ad011b

Coupled-generalized nonlinear Schrödinger equations solved by adaptive step-size methods in interaction picture

Lei Chen(陈磊), Pan Li(李磐), He-Shan Liu(刘河山), Jin Yu(余锦), Chang-Jun Ke(柯常军), and Zi-Ren Luo(罗子人)
Chin. Phys. B, 2023, 32 (**2**): 024213. DOI: 10.1088/1674-1056/ac76a8

Controlled propagation and particle manipulation of off-axis-rotating elliptical Gaussian beams in strong nonlocal media

Rong-Quan Chen(陈荣泉)[1], Rui-Lin Xiao(肖瑞林)[2,†], Wei Wang(王伟)[1], Xi-Xi Chu(储茜茜)[1], Yu-Qing Song(宋雨晴)[1], Xu-Dong Hu(胡旭东)[1], and Ming Chen(陈明)[1,‡]

[1] *Guangxi Key Laboratory of Optoelectronic Information Processing, School of Optoelectronic Engineering, Guilin University of Electronic Technology, Guilin* 541004, *China*

[2] *School of Physics, Anshan Normal University, Anshan* 114007, *China*

(Received 6 December 2024; revised manuscript received 8 January 2025; accepted manuscript online 14 January 2025)

Off-axis-rotating elliptical Gaussian beams (OareGB) oblique incidence in strong nonlocal medium exhibit novel propagation properties. The analytical expressions of semi-axial beam widths, and center-of-mass trajectory equations for transmitting off-axis-rotating elliptical Gaussian beams in strong nonlocal media are obtained using the *ABCD* transfer matrix method. The study revealed that the trajectory of the mass's center in the cross-section can be controlled by changing the sizes of the OareGB parameters c, d, ζ, and f. The gradient force of the light field causes the spot region to form a spatial potential well in the media, and this spatial potential well can effectively capture nanoparticles. The particles captured by the light field can move along with the beam, realizing the effective manipulation of the particle trajectory. These laws may be applied to modulating the propagation path of light beams and optical tweezer technology.

Keywords: nonlinear optics, off-axis-rotating elliptical Gaussian beam, orbital angular momentum

PACS: 42.25.Bs, 42.65.–k, 42.65.Tg

DOI: 10.1088/1674-1056/ada9dd **CSTR:** 32038.14.CPB.ada9dd

1. Introduction

The conventional vortex beams have phase singularities and exhibit hollow phase structures,[1] such as the superimposed chirped Bessel–Gaussian vortex soliton,[2] and circular Airy Gaussian vortex soliton.[3] There is, however, another kind of vortex-free beam that can also carry OAMs, which is an elliptic Gaussian beam with a cross-phase.[4] Literature[5] theoretically demonstrated that spiral elliptic solitons can exist in a nonlocal nonlinear model with thermal nonlinearity and experimentally observed the stable propagation of such solitons in the lead glass. In practice, an off-axis vortex beam is obtained when the center of the incident beam is shifted from the center of the spiral phase plate (SPP).[6] The initial position of the vortex center gives a linear transverse displacement of the beam during propagation through the medium,[7] which changes the initial orbital angular momentum carried by the vortex beam. Based on the experiments, manipulations of the size and rotation direction of the multiple off-axis hollow-structured vortice optical fields were realized.[8] The modulation effect of the multi-off-axis vortex phase on the Laguerres–Gaussian beam was reported in Ref. [9], resulting in multi-lobe and multi-ring structured light intensity. Most studies are concerned with the propagation of beams perpendicularly incident to the medium, and the propagation of beams inclined to the medium has been less studied. The authors in Ref. [10] reported that the direction of the dovetail beam incident on the photorefractive crystal was changed to control its output position.

On the other hand, the optical intensity gradient force has a wide range of applications in the fields of micro-nano manipulation and particle capture.[11] Optical gradient force is a kind of force generated when light interacts with matter, which is affected by light intensity gradient and refractive index. In 2018, Hadad *et al.* proved experimentally that helical beams can capture particles, which make the particles show axial rotational motion, realizing the famous Archimedean helix.[12] Thus far, structured light beams with customized phase and amplitude have been successfully applied to drive the optical transport of particles in three-dimensional (3D) trajectories by exerting optical forces arising from high intensity and phase gradients.[13,14]

In this paper, the influence of changing the beam incidence direction and off-axis parameters on the transmission trajectory is considered. The off-axis-rotating elliptical Gaussian beam (OareGB) oblique incident in a strong nonlocal nonlinear medium (SNNM) is found to be stably transmitted by using the ABCD transfer matrix method[15] for the analytical study, and the split-step fourier method for the numerical simulation. The center-of-mass trajectory, orbital angular momentum, and beamwidth of the OareGB are changed by varying the incident direction, cross-correlation coefficient, and off-axis position. The direction of the Poynting vector determines

†Corresponding author. E-mail: xiaoruilin0797@163.com

‡Corresponding author. E-mail: mchenqq2011@163.com

© 2025 Chinese Physical Society and IOP Publishing Ltd. All rights, including for text and data mining, AI training, and similar technologies, are reserved.

the direction of the energy flow, the center of mass moves in the same direction as the energy flow, and the optical intensity gradient force of the OareGB can effectively capture Rayleigh particles in the vicinity of the center of mass.

2. Theoretical model

When the dispersion broadening effect and the nonlinear compression effect are accurately balanced, the beam can maintain a stable waveform in the nonlocal nonlinear media, forming optical solitons. OareGB propagation in SNNM satisfies the Snyder–Mitchell model[16]

$$\mathrm{i}\frac{\partial\varphi}{\partial z}+\frac{1}{2}\left(\frac{\partial^2}{\partial x^2}+\frac{\partial^2}{\partial y^2}\right)\varphi-\frac{1}{2}\gamma^2P_0(x^2+y^2)\varphi=0. \tag{1}$$

It should be noted that equation (1) as well as the following calculations are all in the dimensionless system after the variable transformation of $x=X/w_0$, $y=Y/w_0$, $z=Z/Z_r$, where X,Y,Z are the coordinates in laboratory system, and $Z_r=kw_0^2$ is the diffraction length of paraxial beam, w_0 being the initial beam width of paraxial beam φ. The function of OareGB can be expressed as

$$\begin{aligned}\varphi(x_0,y_0,0) &= A_0\exp\left\{-\left[\frac{(x_0+c)^2}{2a^2}+\frac{(y_0+d)^2}{2b^2}\right]\right\}\\ &\times\exp[\mathrm{i}\Omega(x_0+c)(y_0+d)]\\ &\times\exp(\mathrm{i}\zeta x_0+\mathrm{i}fy_0),\end{aligned} \tag{2}$$

where A_0 is the amplitude, a and b are the light intensity distribution parameters, c and d are off-axis parameters characterizing the position of the light intensity center, ζ and f are the slope of the projected trajectory of the mass's center on the x–z plane about the Z-axis and the slope of the projected trajectory of the mass's center on the y–z plane about the Z-axis, respectively, which characterize the direction of incidence of the soliton.[17] Where $\gamma=1/(\sqrt{2\pi}w_m^2)$,[16] and $(x_\mathrm{c},y_\mathrm{c})$ is coordinate of the mass's center, P_0 is the beam power, M is orbital angular momentum of optical beam[18,19]

$$x_\mathrm{c}=\frac{\int_{-\infty}^{+\infty}\int_{-\infty}^{+\infty}x|\varphi|^2\mathrm{d}x\mathrm{d}y}{\int_{-\infty}^{+\infty}\int_{-\infty}^{+\infty}|\varphi|^2\mathrm{d}x\mathrm{d}y}, \tag{3}$$

$$y_\mathrm{c}=\frac{\int_{-\infty}^{+\infty}\int_{-\infty}^{+\infty}y|\varphi|^2\mathrm{d}x\mathrm{d}y}{\int_{-\infty}^{+\infty}\int_{-\infty}^{+\infty}|\varphi|^2\mathrm{d}x\mathrm{d}y}, \tag{4}$$

$$P_0=\int_{-\infty}^{+\infty}\int_{-\infty}^{+\infty}|\varphi_0|^2\mathrm{d}x\mathrm{d}y=\pi abA_0^2, \tag{5}$$

$$\begin{aligned}M &= \mathrm{Im}\int_{-\infty}^{+\infty}\int_{-\infty}^{+\infty}\varphi^*\left(x\frac{\partial\varphi}{\partial y}-y\frac{\partial\varphi}{\partial x}\right)\mathrm{d}x\mathrm{d}y\\ &= \frac{1}{2}P_0\left[-2cf+2d\zeta+(a^2-b^2)\Omega\right].\end{aligned} \tag{6}$$

The propagation of OareGB in the ABCD optical system can be dealt with by the Collins equation

$$\begin{aligned}\varphi(x,y,z) &= -\frac{\mathrm{i}\sqrt{\gamma^2P_0}}{2\pi\sin(\sqrt{\gamma^2P_0}z)}\\ &\times\exp\left[\frac{\mathrm{i}\sqrt{\gamma^2P_0}(x^2+y^2)}{2\tan(\sqrt{\gamma^2P_0}z)}\right]\\ &\times\iint\varphi(x_0,y_0)\exp\left[\frac{\mathrm{i}\sqrt{\gamma^2P_0}}{2\tan(\sqrt{\gamma^2P_0}z)}(x_0^2+y_0^2)\right.\\ &\left.-\frac{\mathrm{i}\sqrt{\gamma^2P_0}}{\sin(\sqrt{\gamma^2P_0}z)}(xx_0+yy_0)\right]\mathrm{d}x_0\mathrm{d}y_0.\end{aligned} \tag{7}$$

We take the method of Ref. [20] to calculate the cross-term beam width

$$w_{xy}=H_1A^2+H_2AB+H_3B^2-x_\mathrm{c}y_\mathrm{c}, \tag{8}$$

where

$$H_1=\frac{\int_{-\infty}^{+\infty}x_0y_0|\varphi_0(x,y)|^2\mathrm{d}x_0\mathrm{d}y_0}{\int_{-\infty}^{\infty}|\varphi_0(x,y)|^2\mathrm{d}x_0\mathrm{d}y_0}, \tag{9}$$

$$\begin{aligned}H_2 &= \frac{\int_{-\infty}^{+\infty}x_0\dfrac{\partial\phi_0}{\partial y_0}|\psi_0(x,y)|^2\mathrm{d}x_0\mathrm{d}y_0}{\int_{-\infty}^{\infty}|\varphi_0(x,y)|^2\mathrm{d}x_0\mathrm{d}y_0}\\ &+\frac{\int_{-\infty}^{+\infty}y_0\dfrac{\partial\phi_0}{\partial x_0}|\psi_0(x,y)|^2\mathrm{d}x_0\mathrm{d}y_0}{\int_{-\infty}^{\infty}|\varphi_0(x,y)|^2\mathrm{d}x_0\mathrm{d}y_0},\end{aligned} \tag{10}$$

$$H_3=\frac{\int_{-\infty}^{+\infty}\dfrac{\partial\varphi_0(x,y)}{\partial x_0}\dfrac{\partial\varphi_0{}^*(x,y)}{\partial y_0}\mathrm{d}x_0\mathrm{d}y_0}{\int_{-\infty}^{\infty}|\varphi_0(x,y)|^2\mathrm{d}x_0\mathrm{d}y_0}. \tag{11}$$

After a series of calculations, the second-order beam width in the x-direction w_x, in the y-direction w_y, and the cross-term beam width w_{xy} are obtained

$$w_x=\sqrt{\frac{1}{2}a^2\cos^2(\beta)+\frac{(1+a^2b^2\Omega^2)\sin^2(\beta)}{2a^2R}}, \tag{12}$$

$$w_y=\sqrt{\frac{1}{2}b^2\cos^2(\beta)+\frac{(1+a^2b^2\Omega^2)\sin^2(\beta)}{2b^2R}}, \tag{13}$$

$$w_{xy}=\frac{(a^2+b^2)\Omega\sin(2\beta)}{4\sqrt{R}}, \tag{14}$$

where $\beta=\sqrt{\gamma^2P_0}z$, $R=\gamma^2P_0$. The semi-major axis w_a and semi-minor axis w_b of the beam can be expressed as

$$w_a=\sqrt{2}\sqrt{w_x^2+\sqrt{4w_{xy}^2+(w_x^2-w_y^2)^2}+w_y^2}, \tag{15}$$

$$w_b=\sqrt{2}\sqrt{w_x^2-\sqrt{4w_{xy}^2+(w_x^2-w_y^2)^2}+w_y^2}. \tag{16}$$

Substituting Eqs. (12)–(14) into Eqs. (15) and (16), respectively, we can obtain

$$w_a = \sqrt{(a^2+b^2)[\cos^2(\beta)+g\sin^2(\beta)] + \sqrt{(a^2-b^2)^2[\cos^2(\beta)-g\sin^2(\beta)]^2 + h\sin^2(2\beta)}}, \tag{17}$$

$$w_b = \sqrt{(a^2+b^2)[\cos^2(\beta)+g\sin^2(\beta)] - \sqrt{(a^2-b^2)^2[\cos^2(\beta)-g\sin^2(\beta)]^2 + h\sin^2(2\beta)}}, \tag{18}$$

where $g=(1+a^2b^2\Omega^2)/a^2b^2R$, $h=(a^2+b^2)^2\Omega^2/R$, a coordinate rotation through angle θ, which satisfies the following equation:

$$\tan 2\theta = \frac{2w_{xy}}{w_x^2-w_y^2} = \frac{a^2b^2(a^2+b^2)\Omega\sqrt{R}\sin(2\beta)}{(a^2-b^2)[a^2b^2R\cos^2(\beta)-(1+a^2b^2\Omega^2)\sin^2(\beta)]}. \tag{19}$$

Rotational angular velocity

$$\omega_o = \frac{d\theta}{dz} = \frac{1}{2[1+\tan^2(2\theta)]}\frac{d}{dz}\left(\frac{2w_{xy}}{w_{xx}-w_{yy}}\right),$$

we can obtain that

$$\omega_o = \frac{a^2b^2(a^4-b^4)R\Omega\{1+a^2b^2(R+\Omega)+[-1+a^2b^2(R-\Omega^2)]\cos(2\beta)\}}{2\{(a^2-b^2)^2[a^2b^2R\cos^2(\beta)-(1+a^2b^2\Omega^2)\sin^2(\beta)]^2 + a^4b^4(a^2+b^2)^2R\Omega^2\sin^2(2\beta)\}}. \tag{20}$$

When $\partial w_a/\partial z=0$ and $\partial w_b/\partial z=0$, we can obtain the critical power

$$P_c = \frac{(a^2+b^2)^2}{4a^4b^4\gamma^2}, \tag{21}$$

and critical coefficient of cross-term

$$\Omega_c = \frac{a^2-b^2}{2a^2b^2}. \tag{22}$$

Equation (17) is simplified as $w_{ca}=\sqrt{2}a$, equation (18) is simplified as $w_{cb}=\sqrt{2}b$. From Eqs. (17) and (18), it is clear that the parameters ζ and f do not affect the size of the semi-major axis and semi-minor axis. When $P_0=P_c$ and $\Omega_0=\Omega_c$, the semi-major axis and semi-minor axis remain constant, independent of the propagational distance z. The critical rotational angular velocity $\omega_c=(a^2+b^2)/(2a^2b^2)$, the period of rotation $T_c=2\pi/\omega_c=4\pi a^2b^2/(a^2+b^2)$.

The trajectory of the mass's center projected in the x–y plane after OareGB passes through the *ABCD* optical system[20] can be expressed as

$$x_c = -c\cdot\cos(\beta)+\zeta\cdot\frac{\sin(\beta)}{\sqrt{R}}, \tag{23}$$

$$y_c = -d\cdot\cos(\beta)+f\cdot\frac{\sin(\beta)}{\sqrt{R}}. \tag{24}$$

The distance of the mass's center from the z-axis can be expressed as

$$r = \sqrt{x_c^2+y_c^2} = \sqrt{(c^2+d^2)R\cos^2(\beta)-\sqrt{R}(df+c\zeta)\sin(2\beta)+(f^2+\zeta^2)\sin^2(\beta)}/\sqrt{R}. \tag{25}$$

According to Eqs. (23) and (24), the trajectory of the mass's center can be obtained as an elliptic equation

$$\begin{aligned} &x_c^2(f^2+d^2R)-2x_cy_c(cdR+f\zeta)+y_c^2(c^2R+\zeta^2)\\ &=(cf-d\zeta)^2. \end{aligned} \tag{26}$$

According to Eq. (17), (18), and (26) it can be seen that the parameters ζ and f only affect the trajectory of the mass's center and do not affect the size of the beam width. Assuming that the angle of rotation of the center of mass around the origin is α, the tangent of α is given by

$$\tan\alpha = \frac{y_c}{x_c} = \frac{d\sqrt{R}\cos(\beta)-f\sqrt{R}\sin(\beta)}{c\sqrt{R}\cos(\beta)-\zeta\sqrt{R}\sin(\beta)}. \tag{27}$$

Revolution angular velocity

$$\begin{aligned} \omega_e &= \frac{d\alpha}{dz} = \frac{1}{1+\tan^2(\alpha)}\frac{d}{dz}\left(\frac{y_c}{x_c}\right)\\ &= \frac{R(-cf+d\zeta)}{(c^2+d^2)R\cos^2(\beta)+(f^2+\zeta^2)\sin^2(\beta)-\sqrt{R}(df+c\zeta)\sin(2\beta)}. \end{aligned} \tag{28}$$

When $\omega_o=\omega_e$, it is satisfied that $\zeta=(a^2+b^2)d/(2a^2b^2)$ and $f=-(a^2+b^2)c/2a^2b^2$.

3. Numerical simulation results and analysis

3.1. Off-axis-rotating elliptic Gaussian optical solitons

We numerically simulate the propagation characteristics of OareGBs in SNNMs using the split-step fourier method to analyze the beam evolution properties.

From Figs. 1(a) and 1(b), the beam spot size remains constant and the phase structure is rotated. Figure 1(c) depicts the Poynting vector[21] $\boldsymbol{S}_\perp = \mathrm{i}(\varphi^*\nabla_\perp\varphi - \varphi\nabla_\perp\varphi^*)/2$ in the cross-section of the OareGB's propagational direction. When OareGB is propagated stably in SNNM, the phase structure and beamwidth remain constant within one period, and the motion direction of the mass's center is consistent with the direction of the energy flow. It can be understood that the flow of energy causes the mass's center of the light beam to move, and the phase determines the direction of the energy flow.

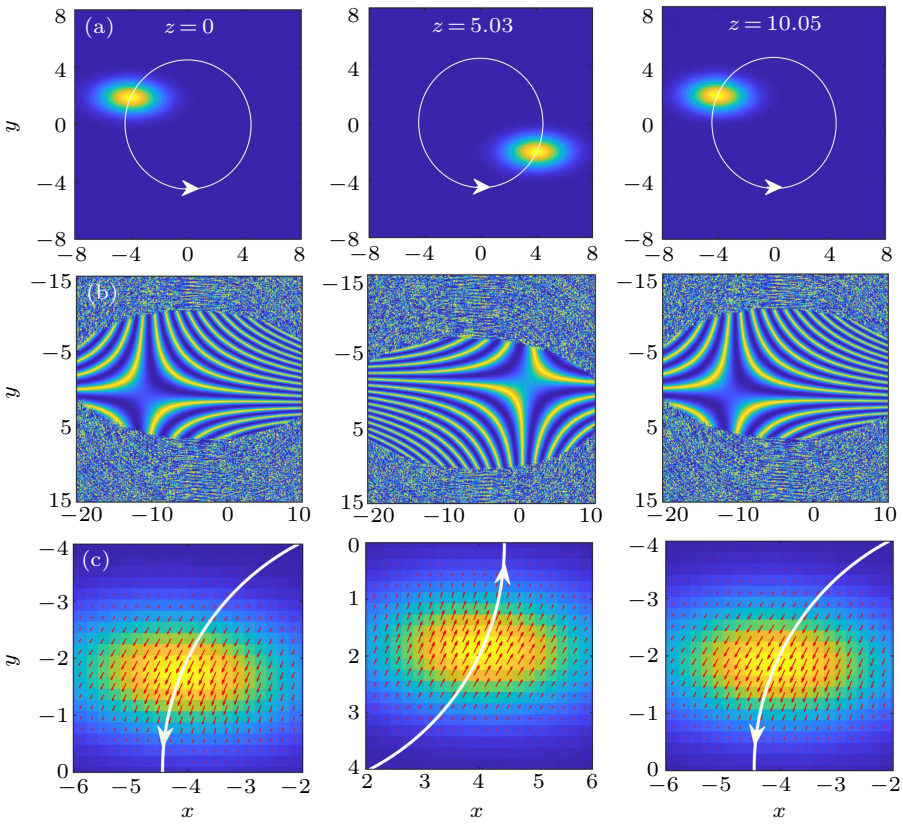


Fig. 1. Propagational characteristics of OareGB. The parameters are chosen as $P_0 = P_c$, $a = 2$, $b = 1$, $c = 4$, $d = 2$, $\Omega = 0.375$, $\zeta = -1.25$, $f = 2.5$, $M = -4.6624$. (a) Trajectory of mass's center (the white line), (b) phase image, (c) energy flow diagram.

3.2. OareGB's breathers

From Fig. 2(b), when the initial power is equal to the critical power, the nonlinear compression effect and the dispersion broadening effect balance each other, the beamwidth size will remain unchanged, and the OareGB soliton has a stable rotational period $z = 10.05$; from Fig. 2(a), when the initial power is smaller than the critical power, the nonlinear compression effect is smaller than the dispersion broadening effect, the beamwidth will first become larger and then smaller, and the rotational period of the mass's center becomes larger ($z = 14.2$). From Fig. 2(c), when the initial power is larger than the critical power, the nonlinear compression effect is larger than the dispersion spreading effect, the beamwidth becomes smaller and then larger, and the rotational period of the mass's center becomes smaller ($z = 7.1$). From Figs. 2(a) and 2(c), it can be seen that the trajectories of the mass's center will be ellipticized when the initial power is not equal to the critical power.

From Fig. 3(a), when $P = P_c$ and $\Omega = 2\Omega_c$, the center of mass radius r and the revolution angular velocity ω_e are constant, but the rotational angular velocity ω_o is variable. From Fig. 3(b), when the light spot is close to the propagational axis (z-axis), the smaller the orbital radius of the mass's center is, the smaller the moment of inertia of the light spot is, and the rotational angular velocity and rotational angular velocity both increase. On the other hand, when the light spot is far away from the propagational axis (z-axis), the larger the orbital radius of the mass's center is, the larger the moment of inertia of the light spot is, and the rotational angular velocity and revolution angular velocity both decrease. This phenomenon shows that the orbital angular momentum of the light spot rotating around the z-axis is conserved. According to Eqs. (17), (18), (20), and Eq. (28), changing the coefficient of the cross-term Ω affects the semi-major axis w_a, the semi-minor axis w_b, and the rotational angular velocity ω_o, but does not affect the revolution angular velocity ω_e. When $\Omega = \Omega_c$, $\zeta = -(a^2+b^2)d/2a^2b^2$, $f = (a^2+b^2)c/2a^2b^2$, $\omega_o = -\omega_e$ is obtained.

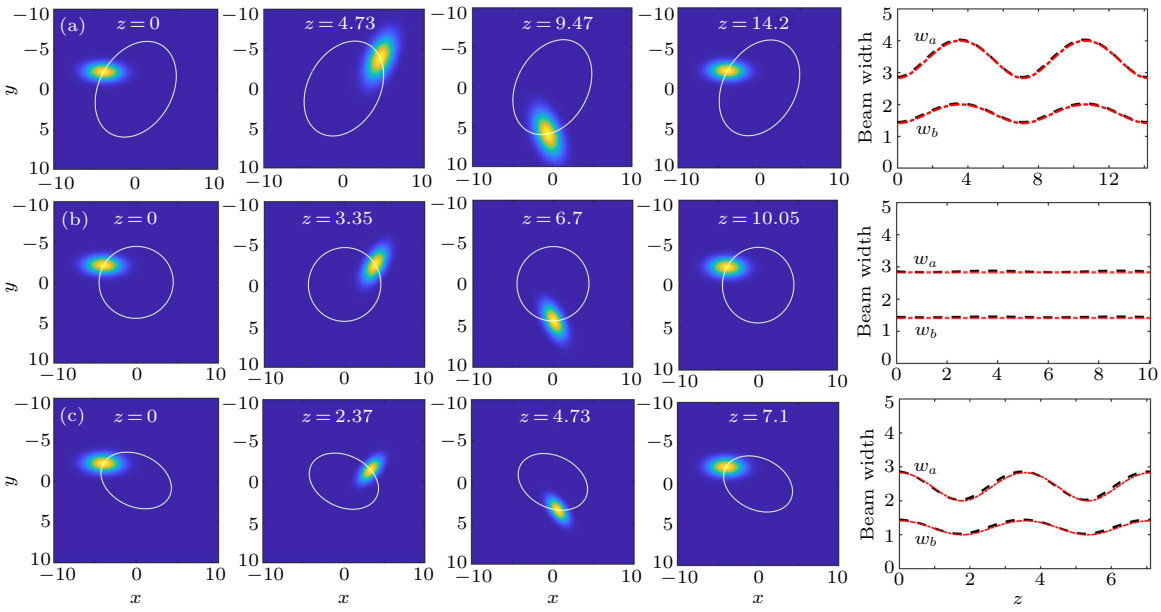


Fig. 2. Comparisons of analytical solution (red dot line) with numerical simulation (black dotted line) for the semi-axes w_a and w_b, with parameters $a=2$, $b=1$, $c=4$, $d=2$, $\Omega=0.375$, $\zeta=1.25$, $f=-2.5$. (a) $P_0=0.5P_c$, $M=2.5508$; (b) $P_0=P_c$, $M=5.1016$; (c) $P_0=2P_c$, $M=10.2032$.

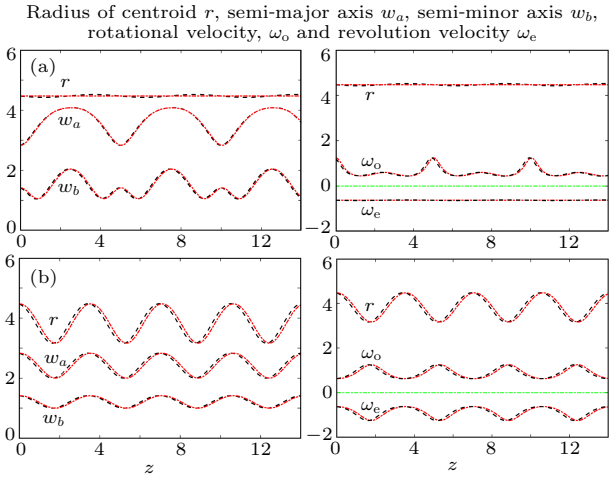


Fig. 3. Comparisons of analytical solution (red dot line) with numerical simulation (black dotted line) for the radius, semi-axes, angular rotation velocity, and angular revolution velocity: (a) the first row, $a=2$, $b=1$, $c=4$, $d=2$, $\Omega=0.75$, $\zeta=-1.25$, $f=2.5$, $P_0=P_c$, $M=-4.4426$; (b) the second row, $a=2$, $b=1$, $c=4$, $d=2$, $\Omega=0.375$, $\zeta=-1.25$, $f=2.5$, $P_0=2P_c$, $M=-9.3248$.

3.3. The gradient force for OareGBs

In general, a particle displays a positive polarizability (PP) whenever its refractive index exceeds that of the background medium, while in the converse case its polarizability is negative (NP). In the presence of an optical field, a particle experiences the gradient force[22]

$$f=\kappa\nabla|\varphi|^2, \tag{29}$$

where κ is a dimensionless quantity, which is related to the refractive index, the radius, and the effective polarizability of the particle. When the refractive index of particle is larger than that of medium, $\kappa>0$, and the particle will be subjected to the gradient force directed at the maximum value of intensity. When the wavelength of the wave is much larger than the size of the particles, Rayleigh scattering occurs, in which nanoparticles are subjected to gradient force f and scattering force $f_{sc}=I\sigma n_b/c$[23] in the medium.where σ is the scattering cross section of the particle, I is the optical intensity, n_b is the refractive index of the surrounding medium.

The gradient force pushes particles towards the central region of the laser beam, while in the PP medium, the scattering force guides particles along the optical axis, leading to nonlocal dynamic self-guidance of light in the medium.[24,25] The gradient force may play a dominant role in optical nonlinearity, especially when the scattering force of nanoparticles can be neglected.[24,26] Since the gradient force and the scattering force are orthogonal and do not interact with each other, only the effect of the gradient force on nanoparticles is taken into account for simplicity. The x-direction gradient force f_x, the y-direction gradient force f_y, and the gradient force f_g and the particle unit mass m_0 can be expressed as follows:

$$f_x=-\frac{(a^2+b^2)^2(c+x)\exp[-(c+x)^2a^{-2}]}{2a^7b^5\pi\gamma^2}, \tag{30}$$

$$f_y=-\frac{(a^2+b^2)^2(d+y)\exp[-(d+y)^2b^{-2}]}{2a^5b^7\pi\gamma^2}, \tag{31}$$

$$f_g=\sqrt{f_x^2+f_y^2}, \tag{32}$$

$$m_0=P_c a c^{-3}. \tag{33}$$

According to $\mathrm{d}f_x/\mathrm{d}x=0$ and $\mathrm{d}f_y/\mathrm{d}y=0$, the maximum values of the gradient force in the x direction $M(f_x)$ and in the y direction $M(f_y)$ can be expressed respectively as follows:

$$M(f_x)=-\frac{\sqrt{2}(a^2+b^2)^2\exp(-1/2)}{4a^6b^5\pi\gamma^2}, \tag{34}$$

$$M(f_y) = -\frac{\sqrt{2}(a^2+b^2)^2 \exp(-1/2)}{4b^6 a^5 \pi \gamma^2}. \tag{35}$$

According to Eqs. (34) and (35), the ratio of $M(f_x)$ to $M(f_y)$ is b/a.

As depicted in Fig. 4, the direction of the gradient force points toward the mass's center. At the position of the mass's center, the gradient force is zero $(f_x = 0, f_y = 0)$, placing particles in an equilibrium state at this position. Under the influence of this force, a spatial potential well forms around the mass's center that can be utilized to capture nanoparticles. Once captured, the nanoparticle is confined within this potential well and exhibits oscillatory motion near the mass's center. As depicted in Fig. 5, the particle vibrates near the mass's center while following its rotation around the z-axis. As nanoparticle position changes within its potential well, gradient forces pull it back toward its position relative to its mass's center. It causes the particle to move with its mass's center in space-a phenomenon akin to manipulating particles using optical tweezers. The spin during propagation along the z-axis leads to continuous changes in gradient force direction and magnitude-resulting in increasingly complex particle trajectories.

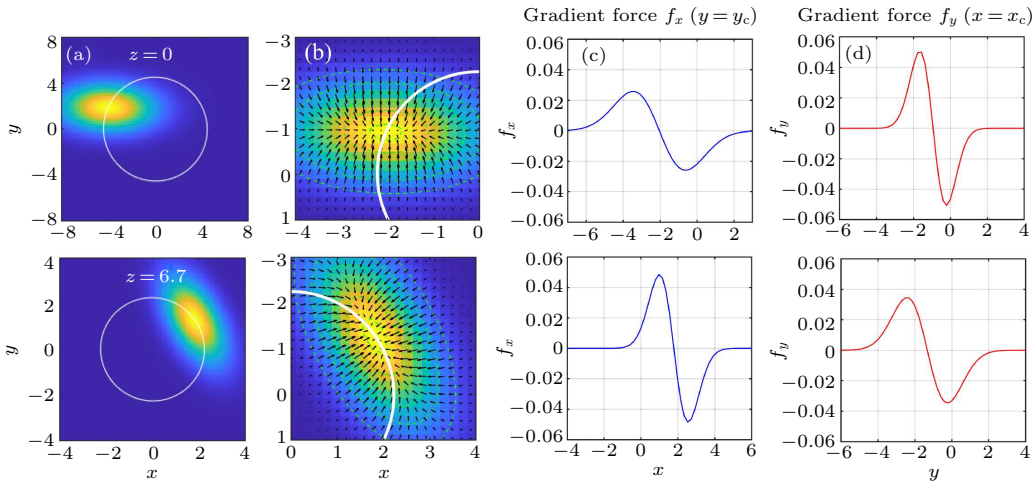


Fig. 4. The gradient force of the OareGB in nonlocal media. The parameters are $a = 2$, $b = 1$, $c = 2$, $d = 1$, $\Omega = 0.375$, $\zeta = -0.625$, $f = 1.25$, $P_0 = P_c$, $M = -1.0009$. The white line is the trajectory of the mass's center.

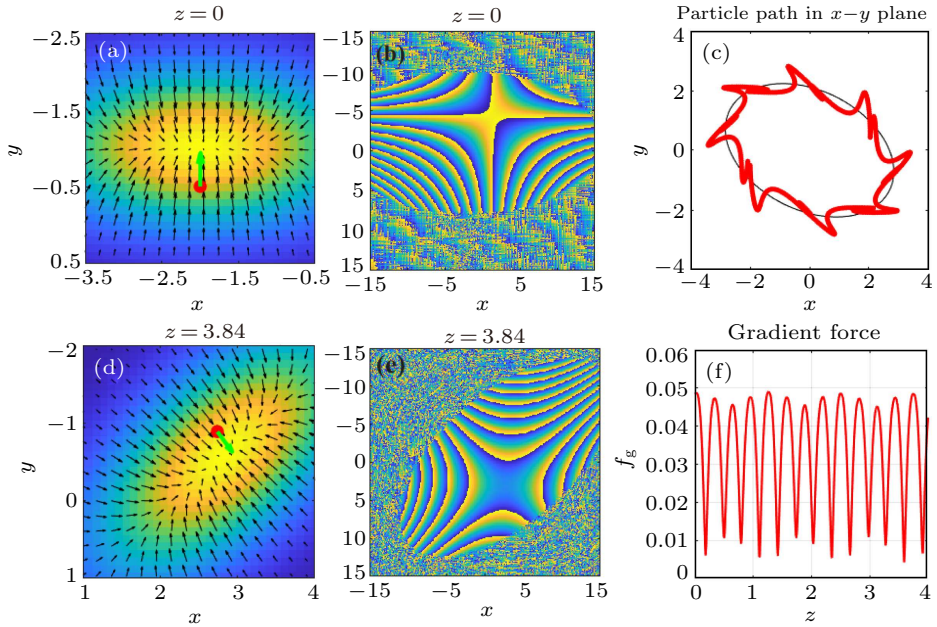


Fig. 5. The variation of gradient force and the particle trajectory. The first column, (a)–(d) the spatial distributions of gradient force (green arrowheads indicate the direction of gradient force); the second column, phase structure (b) and (e); the third column, (c) the particle trajectory (red dotted line) and the trajectory of mass's center (black solid line), and (f) the variation of gradient force. Parameters are chosen as $a = 2$, $b = 1$, $c = 2$, $d = 1$, $\Omega = 0.375$, $\zeta = -1.25$, $f = 1.25$, $P_0 = P_c$, $m = 0.001 m_0$.

From Fig. 6, OareGB maintains stable propagation in SNNM, which must satisfy both $P = P_c$ and the coefficient of cross term $\Omega = \Omega_c$. When the incident direction is fixed, the trajectory of a particle is influenced by factors such as its initial position and mass. As depicted in Figs. 6(a) and 6(b), when the initial position of the particle coincides with the center of the

light beam, it is observed that the gradient force is insufficient to generate significant acceleration for particles with larger masses, ultimately causing them to deviate from their central motion. Consequently, OareGB cannot effectively control the trajectory of heavier particles. Furthermore, as illustrated in Fig. 6(b), when a particle's initial position aligns with the center of the light beam, it becomes evident that the gradient force can produce substantial acceleration for particles with smaller masses, resulting in their confinement near the mass's center. In cases where particles are unable to escape from potential wells within a light field, OareGB induces variable-axis Archimedean spiral motion in these particles. The trajectories of these particles closely mirror those of their light center. Additionally, as shown in Fig. 6(c), greater deviations between a particle's initial position and the center of a light beam lead to increased oscillations at its mass's center. When an initial position strays too far from this central point, OareGB fails to capture these particles effectively. The particles followed a Brownian motion outside the irradiated area and then exhibited a helicoidal motion once they entered the "trapping region".[13]

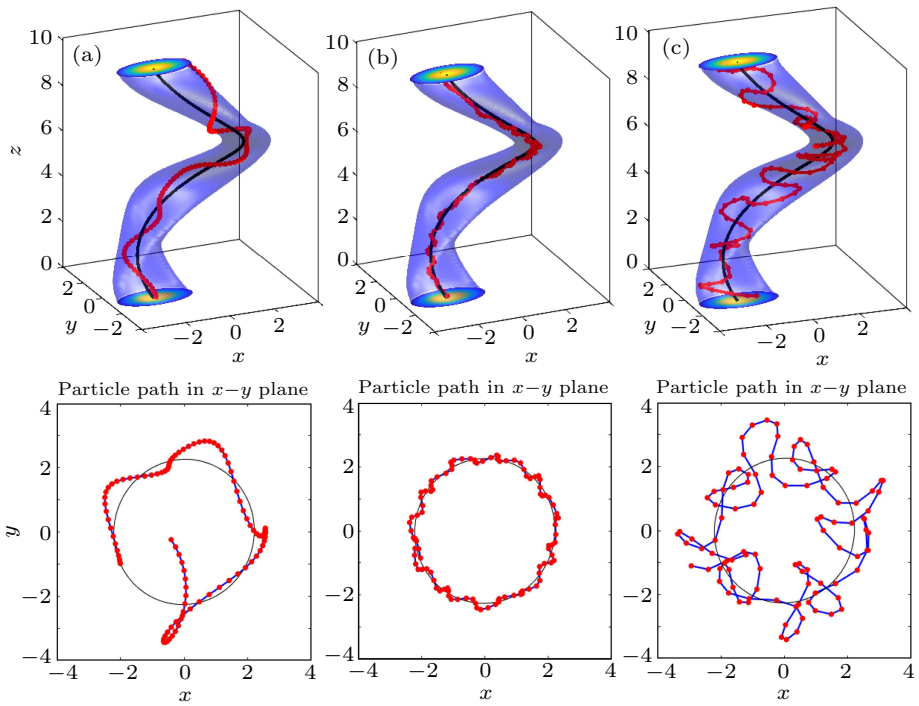


Fig. 6. Three-dimensional light intensity distribution and particle capture. Parameters are chosen as $a = 2$, $b = 1$, $c = 2$, $d = 1$, $\Omega = \Omega_c = 0.75$, $\zeta = -0.625$, $f = 1.25$, $P_0 = P_c$: (a) $m = 0.01m_0$, $x_0 = -2$, $y_0 = -1$; (b) $m = 0.001m_0$, $x_0 = -2$, $y_0 = -1$; (c) $m = 0.001m_0$, $x_0 = -1$, $y_0 = -0.5$. The particle trajectory (red dotted line) and the trajectory of mass's center (black solid line).

4. Conclusion

The semi-axis of the spot can be obtained by the *ABCD* transfer matrix method. The orbital angular momentum M is affected by parameters P_0, a, b, c, d, Ω, ζ, and f. The direction of OareGB's self-rotation can be changed by changing the sign of the cross terms. The direction of the orbit of mass's center around the z-axis depends on the direction of orbital angular momentum M. We can change the off-axis parameter and the incident direction to alter the orbital angular momentum and energy flux of OareGB. The change in energy flux causes the projection of the mass's center to change in the x–y plane. Equation (26) gives the trajectory of the mass's center, and we can obtain any type of orbit by changing the parameters c, d, ζ, and f. Analysis shows that the cross-terms only change the semi-axis length and the rotational angular velocity, but do not change the revolution angular velocity. The spatial potential well formed by the light field of OareGB can effectively capture nanoparticles, allowing particles to move to any position in space. This research has some theoretical reference values for the control of light beam propagation path and particle manipulation.

Acknowledgements

Project supported by the National Natural Science Foundation of China (Grant No. 62075047) and the Natural Science Foundation of Guangxi Zhuang Autonomous Region, China (Grant No. 2020GXNSFDA297019).

References

[1] Wang A, Yu L, Li J and Liang X 2023 *Chin. Phys. B* **32** 044201
[2] Lu Z, Tu J, Zhen W, He S, Wang J, Yan J, Zhang Y and Deng D 2022 *Opt. Commun.* **516** 128238
[3] Liu X, Sun C and Deng D 2021 *Chin. Phys. B* **30** 024202
[4] Kotlyar V V, Kovalev A A and Porfirev A P 2018 *Opt. Express* **26** 141

[5] Liang G, Zhang H, Fang L, Shou Q, Hu W and Guo Q 2020 *Laser Photon. Rev.* **14** 2000141
[6] Kotlyar V V, Kovalev A A and Porfirev A P 2017 *Opt. Lett.* **42** 139
[7] Huang C H, Zheng Y S and Li H Q 2016 *J. Opt. Soc. Am. A* **33** 2137
[8] Geng Y, Hu H, Ma X, Hu X, Chai X, Wang X, Xi S and Zhu Z 2023 *Opt. Express* **31** 27407
[9] Zhang X Y and Xu H F 2024 *J. Opt. Soc. Am. A* **41** 1461
[10] Quan Q, Lian S, Liu Z, Chen H, Yan B and Deng D 2024 *Opt. Lett.* **49** 4585
[11] Yang Y, Ren Y, Chen M, Arita Y and Rosales-Guzmán C 2021 *Adv. Photon.* **3** 034001
[12] Hadad B, Froim S, Nagar H, Admon T, Eliezer Y, Roichman Y and Bahabad A 2018 *Optica* **5** 551
[13] Zhang F, Camarero P, Haro-González P, Labrador-Páez L and Jaque D 2023 *Opto-Electronic Science* **2** 230019
[14] Liu N N, Tang X Y, Liu S Y and Liang Y 2024 *Chin. Phys. B* **33** 054201
[15] Yang Z, Lu D, Hu W, Zheng Y, Gao X and Guo Q 2010 *Phys. Lett. A* **374** 4007
[16] Liang G, Guo Q, Cheng W, Yin N, Wu P and Cao H 2015 *Opt. Express* **23** 24612
[17] Song L, Yang Z, Li X and Zhang S 2018 *Opt. Express* **26** 19182
[18] Wang Q, Mihalache D, Belić M R, Zhang L, Ke L and Zeng L 2022 *Opt. Lett.* **47** 1041
[19] Chen R Q, Chen Y F, Zhang X and Wei J N 2022 *Optik* **271** 170110
[20] Xiao R, Chen R and Chen C 2024 *Opt. Quantum Electron.* **56** 294
[21] Liang G, Shu F, Ma S, Cheng W and Sun C 2023 *New J. Phys.* **25** 033011
[22] Liang G and Wang Q 2021 *New J. Phys.* **23** 103036
[23] Gautam R, Bezryadina A, Xiang Y, Hansson T, Liang Y, Liang G, Lamstein J, Perez N R, Wetzel B, Morandotti R and Chen Z 2020 *Adv. Phys. X* **5** 1778526
[24] Gautam R, Xiang Y, Lamstein J, Liang Y, Bezryadina A, Liang G, Hansson T, Wetzel B, Preece D C, White A, Silverman M, Kazarian S, Xu J, Morandotti R and Chen Z G 2019 *Light Sci. Appl.* **8** 31
[25] Bezryadina A, Hansson T, Gautam R, Wetzel B, Siggins G, Kalmbach A, Lamstein J, Gallardo D, Carpenter E J, Ichimura A, Morandotti R and Chen Z 2017 *Phys. Rev. Lett.* **119** 058101
[26] Xu H, Alvaro P, Xiang Y, Kelly T S, Ren Y X, Zhang C and Chen Z 2019 *Photon. Res.* **7** 28